Applied Catalysis A, General 668 (2023) 119469

Contents lists available at ScienceDirect

Applied Catalysis A, General

journal homepage: www.elsevier.com/locate/apcata

Potassium and cobalt double-doped ferrierites as a new class of soot oxidation catalysts

Gabriela Grzybek [a,*], Magdalena Rudzińska [a], Kinga Góra-Marek [a], Paweł Stelmachowski [a], Grzegorz Słowik [b], Andrzej Kotarba [a]

[a] Faculty of Chemistry, Jagiellonian University in Kraków, Gronostajowa 2, 30–387 Krakow, Poland
[b] Faculty of Chemistry, Maria Curie-Sklodowska University in Lublin, Maria Curie-Sklodowska Sq. 3, 20–031 Lublin, Poland

ARTICLE INFO

Keywords:
Alkali promotion
Cobalt catalyst
Ferrierite
Soot oxidation
Electronic promotion

ABSTRACT

Research efforts to develop an effective soot oxidation catalyst have intensified in recent years due to the increased awareness of the highly harmful effect of soot particles on the human health and the environment. Large-scale application of a developed catalyst calls for a cheap support material allowing for an effective dispersion and thus a decrease in the active phase loading. Zeolites, widely used in catalysis as active phase carriers, possess advantageous characteristics such as a uniform porous structure and large surface area. Furthermore, they are characterized by high availability, good price, and are environmentally friendly. Cobalt-based materials provide promising soot oxidation catalyst phases, and alkali doping can further enhance their activity. This study focuses on the optimization of the potassium loading in the potassium and cobalt double-doped ferrierites towards a new class of cheap and environmentally friendly soot combustion catalysts. The potassium doping of the ferrierite-supported cobalt spienel was optimized in the range of 0–14 wt%. The obtained materials were characterized in terms of their composition (XRF, XPS, XRD, Raman spectroscopy), morphology (SEM, TEM/EDX/FFT), and reducibility (H_2-TPR), and tested in the process of soot oxidation in tight and loose contact modes. The strong promotional effect of potassium was discussed in terms of a significant modification of the catalyst electronic properties (work function studies) and supported by the potassium surface state studies by the alkali thermal desorption method (SR-TAD). It was found that the optimal potassium promoter dispersion leads to the lowest catalyst work function and its highest activity in soot combustion. The effect of nitric oxide was also investigated for selected catalysts. The opposite effect of NO on the activity of undoped and K-doped catalysts was discussed on the basis of in-depth spectroscopic studies. An enhanced formation of nitrate species was found on the surface of the K-containing catalyst which led to the stronger inhibiting effect of NO.

1. Introduction

Incomplete combustion of fossil and bio-derived fuels results in the emission of soot particles, which can enter into the human body, through the respiratory system, or even through the skin, causing many illnesses and cancerogenic changes [1]. Therefore, scientists are looking for solutions that can efficiently reduce soot release into the atmosphere. Effective removal of soot can be achieved by burning it with the use of a catalyst ensuring a satisfactory temperature window of the process. Soot oxidation catalysts can be grouped as noble metal-based catalysts, with emphasis on Pt-based catalysts [2–4], and transition metal oxide-based catalysts (e.g. perovskites, spinels, tunneled and/or layered structures) [5–11]. Among all the reported materials, platinum-based catalysts supported by ceria are the most active ones. However, following the current trend of targeting low-priced noble-metal-free catalysts, transition-metal oxides are gaining considerable attention as promising active phases, whose performance may be significantly improved by the optimized promotion with alkali [7,12,13].

Alkali addition affects the mechanism of soot combustion, strongly modifying the electronic properties of metal oxide catalysts [14,15]. Alkali adsorption on the surface of metal oxides results in a decrease in the work function (WF, φ) of the materials according to the Topping equation (Eq. 1), with the local minimum corresponding to the optimum alkali loading [7]. This minimum correlates with the maximum activity

* Corresponding author.
E-mail address: g.grzybek@uj.edu.pl (G. Grzybek).

https://doi.org/10.1016/j.apcata.2023.119469
Received 1 August 2023; Received in revised form 27 September 2023; Accepted 22 October 2023
Available online 24 October 2023

in the soot combustion for many transition metal-based catalysts [7,14, 16].

$$\Delta\varphi = \frac{4\pi\sigma\mu}{1 + 9\alpha\delta^{3/2}} \quad (1)$$

where: μ - dipole moment of the individual adsorbate, σ - surface concentration of the dipoles, α - adsorbate polarizability.

To increase the effectivity of the catalysts, the active phases are often dispersed on carriers characterized by a high specific surface area. In the case of soot combustion catalysts, mainly ceria, zirconia, alumina, and silica were used [5–7,10]. Surprisingly, mesoporous zeolitic materials, although popular in catalysis, were not widely explored as supports for the soot combustion catalysts. There are only a few papers addressing zeolite-based soot combustion catalysts. It was shown that a promising catalytic activity of Pt catalysts supported on zeolites such as TS-1, H-ZSM5, and USY can be achieved [2–4].

Notably, zeolites are widely used as molecular sieves, adsorbents, detergents, and catalyst supports, but also as catalysts themselves [17–21]. Zeolites-based catalysts are intensively studied for applications in petrochemistry, biomass conversion, environmental catalysis (i.e. NOx removal, CO_2 capture, and conversion), or in lithium-ion batteries [17,22–26]. In our previous paper, we have shown that very active catalysts for steam reforming of ethanol (ESR) can be developed based on zeolites [27]. The cobalt catalyst based on high-silica and pure silica nanometric ZSM-5 zeolite supports indicated extraordinary performance (high selectivity and stability) in the ESR reaction, corresponding to a relatively low degree of carbon deposit formation over the catalysts. Furthermore, the carbon deposit formed during the ESR process was relatively easy to remove under oxidation conditions giving premises for the promising catalytic activity of catalysts in the combustion of carbonaceous materials such as soot particles.

Thus, in this work, we aimed to investigate whether the ferrierite zeolite materials (FER) are suitable candidates as supports for soot combustion catalysts. We prepared a series of cobalt-containing zeolite materials doped with potassium in the range of 0 – 14 wt percent and characterized them with a wide range of complementary techniques. We tested their catalytic activity in tight and loose contact modes of the soot combustion reaction. Moreover, since NO is often present in the gas feed of exhaust engine gases, its effect on catalyst activity is of vital interest for the soot oxidation process [12,13,28], especially in the loose contact mode, where the contact between the soot and catalyst is limited. Therefore, we also tested the selected catalysts in loose contact mode with NO in the gas stream. The strong promotional effect of potassium on the activity of the ferrierite-supported cobalt catalyst (Co/FER) was discussed in terms of work function changes upon K-loading. We corroborated the relationship of observed activity-electronic properties by potassium surface state studies with the species-resolved thermal alkali desorption method (SR-TAD) [29]. We also compared the effect of NO on the undoped Co/FER and optimized potassium-doped Co/FER catalysts and evaluated the results based on the in-depth spectroscopic studies.

2. Experimental

2.1. Catalyst preparation

A series of potassium-doped cobalt catalysts supported on ferrierite (K Co/FER) were synthesized using the commercial NaKFER zeolite (TOSOH 720KOA). The Co_3O_4 phase was deposited by the incipient wetness impregnation (IWI) method using a water solution of $Co(NO_3)_2$ with an appropriate concentration to obtain about 15 wt% loading of cobalt. The Co/FER sample was next dried in the air at 60 °C for 24 h and calcined in the air at 500 °C for 4 h. In the subsequent step, the potassium promoter in the amount of 0 – 14 wt% was added to Co/FER, also by the IWI method, using KNO_3 aqueous solutions with appropriate concentrations, and dried and calcined again according to the procedure described above. A reference Co-exchanged catalyst, CoFER, was prepared by the ion-exchange of native NaKFER in a 1 M $Co(NO_3)_2$ solution at 80 °C, followed by drying in room temperature and calcination in air at 500 °C for 4 h.

2.2. Materials characterization

The phase composition was examined with the X-ray diffraction method (XRD) using a Rigaku Multiflex X-ray diffractometer. The diffraction patterns were taken using the CuK_α radiation of $\lambda = 1.54$ Å (2 theta between 5° and 90°, step of 0.02°, 2° per minute). Micro-Raman spectroscopy was applied to confirm the spinel structure of the cobalt phase present in the samples (fresh and used catalysts). The Raman spectra (in the range of 100–1000 cm^{-1}, resolution of 1 cm^{-1}) were recorded at room temperature using a Renishaw InVia spectrometer (laser 785 nm). The elemental composition of the obtained catalyst was checked using an X-ray Fluorescence Spectrometer (XRF, ARL QUANT'X). The Rh anode was applied to generate the X-rays of 4 – 50 kV (1 kV step). The texture of the catalysts was analyzed by N_2-physisorption at − 196 °C with a Quantachrome Autosorb-1-MP gas sorption apparatus using the procedure described elsewhere [30].

The Quanta 3D FEG scanning electron microscope (SEM) of the FEI Company was used for sample imaging. The catalyst samples were applied to aluminum supports covered by carbon conductive tape and then transferred to the microscope. Microscopic characterization of the catalysts was carried out at an accelerating voltage of 30 kV. The detailed morphological characterization of the samples was carried out using the scanning transmission electron microscope (TEM, Titan G2 60–300 kV, FEI Company) with an acceleration voltage of the electron beam equal to 300 kV (the experimental details described elsewhere [31]). Information on the distribution of the elements was obtained by energy dispersion X-ray spectroscopy (EDX). The mapping was carried out in the scanning TEM mode (STEM). Phase separation in the cobalt-based catalysts was performed with the fast Fourier transform (FFT) by using masking available in the Gatan Digital Micrograph software package.

Hydrogen temperature programmed reduction (H_2-TPR) was carried out in a fixed-bed quartz flow microreactor system connected to a thermal conductivity detector, TCD (TCD3, Valco, Houston, TX, USA). 50 mg of the sample was placed in the reactor and degassed in a flow of high purity Ar (99.999%) at 550 °C for 30 min. Subsequently, the reactor was cooled to 80 °C and the sample was reduced in a gas mixture of 5 mol% H_2 in Ar (both pure 99.999%) with a 10 ml·min^{-1} flow rate, controlled by the mass flow controller in the temperature range of 80–950 °C with a heating rate of 10 °·min^{-1}. The water produced during the reduction was removed by a cold trap.

Changes in the work function of catalysts due to potassium doping were examined by measuring contact potential difference (CPD) using the Kelvin probe method with a KP6500 device (McAllister Technical Services, Coeurd'Alene, ID, USA). The stainless steel plate (d = 3 mm) was used as a reference electrode ($WF_{ref} = 4.3$ eV). The studies were performed under ambient conditions, with vibration frequency at 114 Hz and amplitude at 40 arb. uni.

The multi-chamber ultra-high vacuum system (PREVAC) was utilized to conduct X-ray photoelectron spectroscopy (XPS) studies, with a hemispherical Scienta R4000 electron analyzer for collecting spectra. Complementary equipment included a Scienta SAX-100 X-ray source (Al Kα, 1486.6 eV, 0.8 eV band) and the XM 650 X-Ray Monochromator (0.2 eV band). For survey spectra, the pass energy of the analyzer was set at 200 eV with a 500 meV step, and for high-resolution spectra (Si 2p, Al 2p, Co 2p, O 1 s, K 2p, N 1 s, and C 1 s), the pass energy was set at 50 eV with a 50–100 meV step. The analysis chamber had a base pressure of $5{\cdot}10^{-9}$ mbar, which did not exceed $3{\cdot}10^{-8}$ mbar during the spectra collection. Data processing was carried out using CasaXPS software (v 2.3.23 PR1.0) [32].

For the IR studies the pristine and reagent-contacted catalysts (5 mg) were mixed with potassium bromide (100 mg) and pressed in the form of thin pellets. IR spectra were acquired in transmission mode with a Bruker Vertex 70 spectrophotometer equipped with an MCT detector that collected 100 scans for each spectrum with 2 cm^{-1} resolution.

2.3. Thermal alkali desorption studies

Alkali promoters are known to desorb from catalyst surfaces in high temperatures. If the loss of the alkali dopant is extensive, the properties of the catalyst will change and its activity usually deteriorates. Thus, detailed studies of the evolution of their surface state are of the greatest importance. As shown in our previous works [29,33,34], it is possible by monitoring the thermal desorption flux of alkali using the species-resolved thermal alkali desorption method (SR-TAD). Upon heating of an alkali-containing catalyst, the energy needed for the alkali desorption (atoms, cations, Rydberg atoms), the temperature range of desorption, and the amount of desorbing individuals can be determined. The analysis of the desorption parameters such as the onset and intensity of desorption flux as well as desorption energies gives information about the alkali chemical state (localization, identification of surface phases containing alkali admixtures), alkali surface dynamics (mobility of alkali), and stability of alkali on the catalyst surface (including mechanism and energy barriers of their escape). The desorption flux of potassium atoms during heating and subsequent cooling of the sample was measured with a surface ionization detector. The experiments were done in a vacuum apparatus (10^{-8} mbar). The pelletized samples (diameter of 13 mm) were heated to 600 °C and then cooled down (rate 10 °C/min) [34,35].

2.4. Catalytic tests

The soot oxidation tests were performed using thermogravimetric analysis using TGA/DSC 1 equipment (Mettler Toledo). The samples for catalytic tests were prepared by mixing (shaking in Eppendorf tube) 50 mg of catalyst and 5 mg of soot for 1 min (loose contact) and grounding the same amounts of sample and soot in an agate mortar for 10 min (tight contact). The prepared mixtures were then placed in an alumina crucible and heated in a flow of 5% O_2/He 60 ml·min^{-1} (mixed with Ar 20 ml·min^{-1}) in a temperature range of 30–900 °C at a heating rate of 10 °C/min.

For the loose contact mode, the effect of NO in the gas stream was investigated by performing temperature-programmed soot oxidation tests in the temperature range of 30–800 °C. The samples were prepared in the same way as for the TGA experiments. Measurements were carried out in a U-shaped quartz reactor using 5% O_2/He and 3.3% O_2/0.33% NO/He gas mixtures with a total flow of 60 ml·min^{-1}. The composition of the gas phase was monitored with a QMS detector (Hiden, lines for CO ($m/z = 28$), CO_2 ($m/z = 44$), NO ($m/z = 30$), and O_2 ($m/z = 32$)).

3. Results and discussion

3.1. Physicochemical characterization of the catalysts

The series of K-doped Co/FER catalysts were characterized in terms of their chemical and phase composition, reducibility, and morphology (XRF XRD, Raman Spectroscopy, H_2-TPR SEM, HR-TEM/EDX/FFT). XRF analysis revealed that the desired loading of the active cobalt phase was successfully achieved at the level of 13.2 ± 2.5 wt% (Table 1). The results also confirmed that we obtained the series of potassium-doped samples with increasing K-loading, in the range of 0–14 wt%. Almost all studied samples contained native potassium located in ion-exchanged positions of the zeolite framework; the potassium content for pure NaKFER zeolitic support determined from XRF studies equaled 5.9 wt%. A lower potassium content in the case of the ion-exchanged CoFER sample can be explained by the potassium replacement with cobalt ions occupying ion-exchange positions [36].

Table 1
Cobalt and potassium content in the studied catalysts from the XRF studies.

Catalyst	Content by weight/%	
	Co	K
CoFER	1.4	2.6
Co/FER	13.9	0*
2 K Co/FER	13.5	1.3*
6 K Co/FER	10.6	5.7*
10 K Co/FER	14.5	10.0*
14 K Co/FER	13.3	13.1*

* The content of potassium was calculated as the difference between the total amount of K and the amount from the undoped Co/FER catalyst.

From the X-ray diffractograms collected in Fig. 1A, it can be inferred that there was no change in the crystal structure of ferrierite support after the addition of cobalt. Both positions and intensities of the diffraction lines representative of the FER structure remained unaffected. The maxima marked by * at 2θ equal to 19.1, 31.3, 36.9, 44.9, 55.7, and 59.4 in the diffractograms of Co/FER and 14 K Co/FER catalysts were identified as corresponding to the (111), (220), (311), (400), (422), and (511) reflection planes of Co_3O_4 (ICSD 69378), respectively. Moreover, no additional reflexes indicating the formation of potassium-originated phases, such as KNO_3, were detected in the XRD pattern of the 14 K Co/FER catalyst, which we selected for XRD studies as a representative K-containing sample, due to its highest content of potassium.

Raman spectra of the selected, Co/FER and 6 K Co/FER, catalysts are shown in Fig. 1B. Five bands located at 187 (F_{2g}), 476 (E_g), 515 (F_{2g}), 613 (F_{2g}), and 684 (A_{1g}) cm^{-1} confirmed the presence of the spinel phase.

In the TPR profiles of the catalysts (Fig. 1C), three main maxima at ca. 330, 360, and 410 °C are usually assigned to the $Co^{3+} \rightarrow Co^{2+}$ and $Co^{2+} \rightarrow Co^0$ reduction processes [37]. The presence of three maxima may be explained by two locations of cobalt, in the form of cobalt spinel on the external surface of ferrierite and in the form of Co^{2+} species in ion-exchanged positions. Although almost no change in the reducibility of the active cobalt phase is observed upon the introduction of potassium in the amount of 2 wt% (2 K Co/FER), a substantial change in the reduction profile is observed for the 6 K Co/FER sample. It is illustrated by the shift of the TPR profile by about 40 °C towards higher temperatures and the sharp, intense peak in the range of 400 – 600 °C for the 6 K Co/FER sample. The latter peak was attributed [29] to the nitrates on the surface of the catalyst that originate from the potassium source. In turn, the high-temperature peak (>800 °C) observed for CoFER is typical for reduction of cobalt in ion-exchange positions [30].

The representative SEM images of the zeolite support (NaKFER), Co-exchanged ferrierite (CoFER), and Co and K impregnated ferrierite (Co/FER, 2 K Co/FER, 6 K Co/FER) are shown in Fig. 2.

The morphology of NaKFER (Fig. 2A) and Co-containing catalysts (CoFER, Co/FER, Fig. 2B,C) is characterized by aggregated lamellar and needle-shaped crystallites with irregular sizes and shapes typical of the FER morphology [38–41]. For bare zeolite, the grains are loosely arranged, whereas they are much more compact in the case of Co catalysts; there are no large spaces between the grains, and the grains are much more squeezed together. In the case of potassium-doped samples (Fig. 2D,E) the grains of the catalyst are additionally covered with a phase of an indefinite shape, which also fills the spaces between the grains. The grain boundaries are more difficult to define. These observations are consistent with the observed decrease in the specific surface area upon K-doping (Table S1).

The TEM images together with the complementary phase identification of Co/FER and 6 K Co/FER are presented in Fig. 3. The cobalt spinel nanograins of the size in the range of 10–30 nm are dispersed on the grains of the ferrierite support.

The STEM images together with the complementary EDX elemental

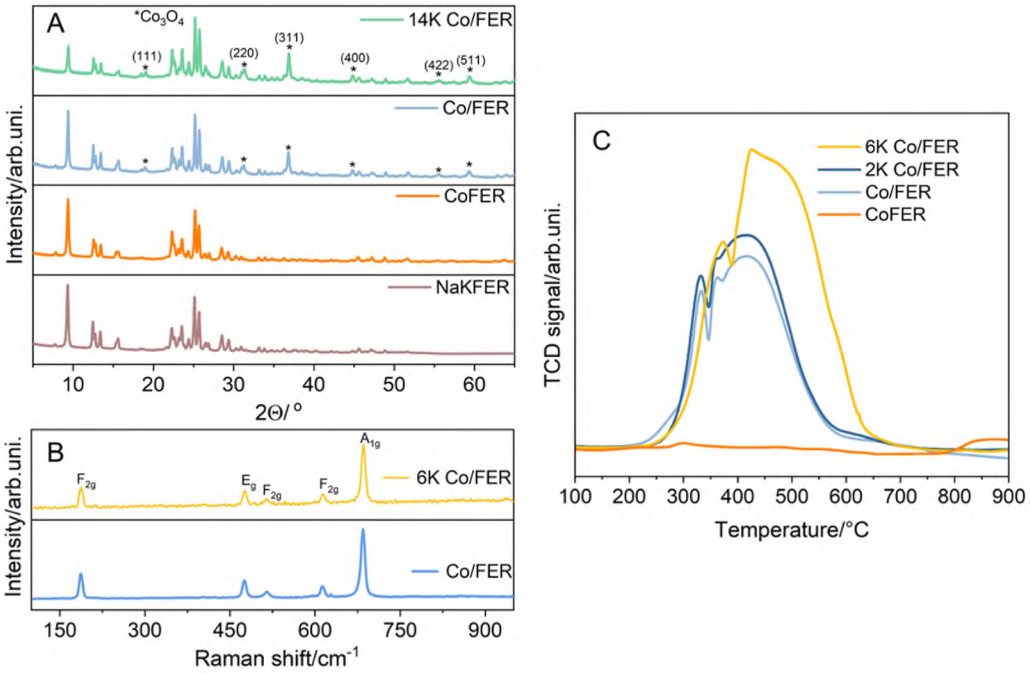

Fig. 1. A) XRD patterns of the NaKFER zeolite support and CoFER, Co/FER, 14 K Co/FER catalysts. B) Raman spectra of the Co/FER and 6 K Co/FER catalysts. C) H_2-TPR profiles of the CoFER, Co/FER, 2 K Co/FER, and 6 K Co/FER catalysts.

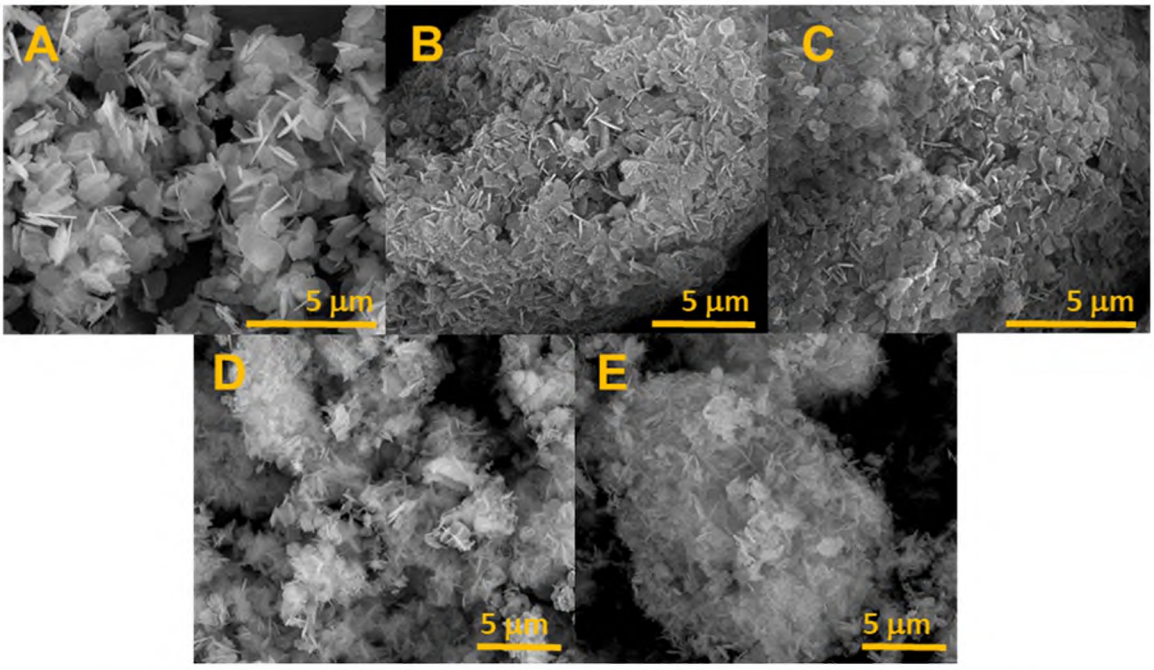

Fig. 2. SEM images of the A – NaKFER, B – CoFER, C – Co/FER, D – 2 K Co/FER, E – 6 K Co/FER catalysts.

maps for NaKFER, CoFER, Co/FER, 2 K Co/FER, and 6 K Co/FER catalysts are presented in Fig. 4. First, the STEM images revealed that the morphology of zeolite is preserved after the introduction of cobalt and potassium. Second, the collected elemental maps revealed the uniform distribution of cobalt on the zeolite support for Co/FER, 2 K Co/FER, and 6 K Co/FER catalysts. Additionally, the cobalt map collected for the CoFER cobalt-exchanged sample indicated a uniform cobalt distribution in the zeolite channels. The potassium maps indicated that it is well distributed on the surfaces of all catalysts.

3.2. *The nature of potassium promotional effect*

In Fig. 5A we compared the activity in the soot combustion reaction, expressed as the temperature of 10%, 50%, and 90% conversion, carried out in tight contact mode for the series of NaKFER, CoFER, Co/FER, and K-doped Co/FER samples. The presented results revealed a negligible activity of bare ferrierite and cobalt-exchanged zeolite. For these samples, soot is oxidized in the same temperature window as for the non-catalytic process.

The Co/FER catalyst containing the cobalt spinel phase segregated

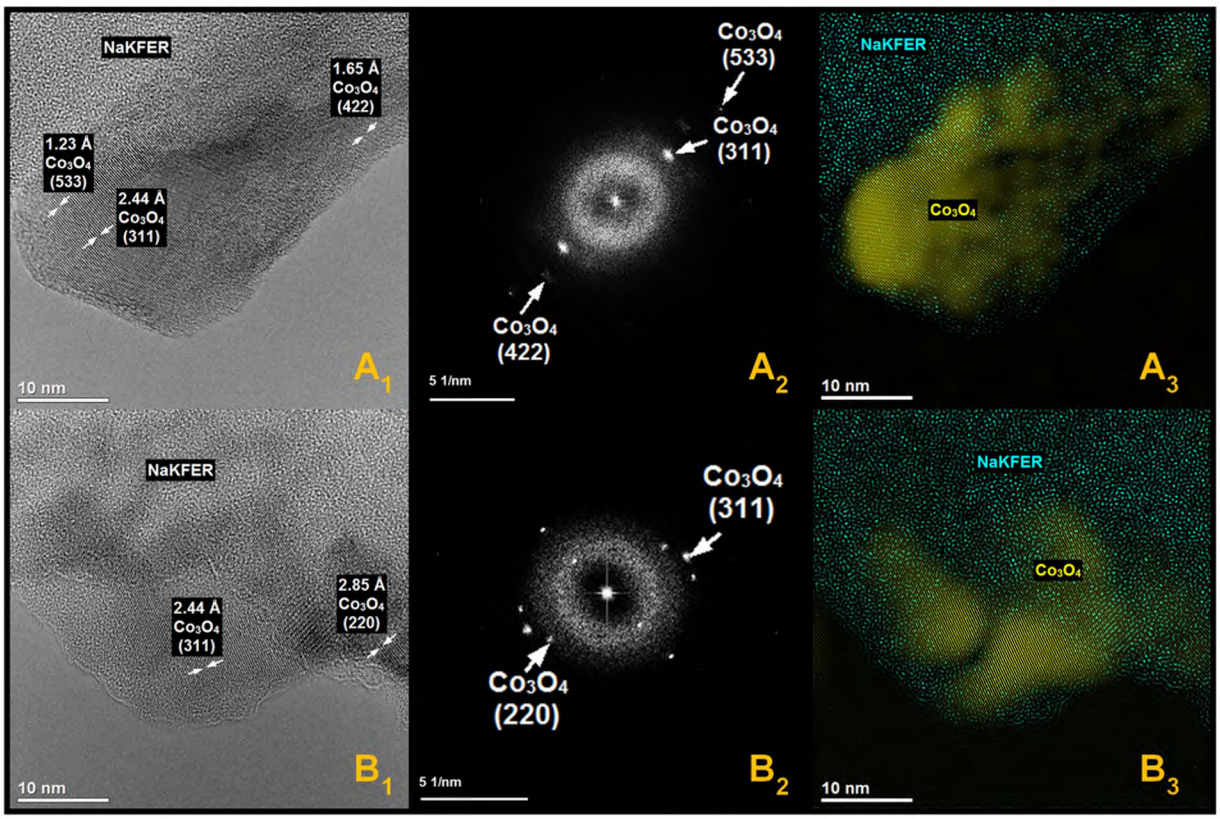

Fig. 3. TEM images with phase identification for the Co/FER (A_1-A_3) and 6 K Co/FER (B_1-B_3) catalysts.

on the external surface of the support exhibited a significantly higher activity with respect to the non-catalytic process. The most significant activity enhancement was observed at the beginning of the process, where $T_{10\%}$ was reduced by about 130 °C, whereas the temperatures of 50% and 90% of conversion were lowered by about 75–80 °C. Most importantly, the addition of potassium promoter significantly improves the activity of the Co/FER catalyst and strongly depends on the K loading. For the 2 K Co/FER sample we observed a $T_{90\%}$ decrease of about 45 °C. The optimal potassium content was found for the 6 K Co/FER sample, for which $T_{90\%}$ equals about 460 °C and corresponds to a 150 °C shift toward lower temperatures. Further increase of K content did not improve the activity of our catalysts, in fact we observed a slight increase in $T_{90\%}$ for 10 K Co/FER and 14 K Co/FER. Moreover, the three subsequent catalytic tests for the most active sample, 6 K Co/FER, indicated its very high stability (Fig. 5B). The catalytic parameters such as $T_{10\%}$, $T_{50\%}$, and $T_{90\%}$ are almost the same for three consecutive soot combustion cycles. The structural and morphological characterization of the used catalyst indicated no significant changes after the stability testing (Fig. S1).

For the selected CoFER, Co/FER, and 6 K Co/FER catalysts, we performed thermogravimetric soot combustion studies in the loose contact mode. These conditions are closer to real-life scenarios, in which the soot is trapped on the catalyst external surface in the exhaust diesel particulate filter. As expected, the activity of all three catalysts, decreased significantly due to limited contact between the soot and catalyst (Fig. 6, S2). However, the general trend in activity is preserved, the comparison of the temperature of 90% conversion indicates a positive effect of potassium in the loose contact mode as well (the full set of the activity parameters is presented in Fig. S2).

For the performed catalytic tests, the mass spectrometry analysis of the outlet gas composition showed almost 100% selectivity to CO_2 (Fig. S3).

According to a recent review on soot combustion [7], the most active catalysts that meet the target conditions for catalytic soot removal are the ones containing noble metals, in particular platinum. However, a recent trend in soot oxidation aims at the development of noble-metal-free catalysts. The most active materials reported in the literature operate in the temperature range of 400–600 °C. Moreover, the tight contact mode performance of our best catalyst, 6 K Co/FER, is at the lower end of this range, approaching the highly active noble-metal catalysts.

3.3. *Analysis of the potassium promotion effect in terms of the catalyst work function changes*

Electronic surface promotion plays a key role in the soot oxidation reaction [7], therefore, we investigated the influence of potassium on the electronic properties of the catalyst by measuring the changes in the work function upon K doping using the Kelvin method. Fig. 7 illustrates similar profiles of the changes in work function and catalytic activity measured in the tight contact mode with the potassium content determined from XRF studies. Both the WF and $T_{90\%}$ data sets show non-monotonous behavior, with a minimum corresponding to the 6 K Co/FER sample. The initial linear decrease in the work function with increasing potassium loading results from surface dipole formation and the resultant increase of the surface electron density. Then, after passing the work function minimum, a further increase in potassium coverage leads to depolarisation and a consequent increase in the work function. The WF minimum, related to the optimal dispersion of the potassium species forming surface dipoles, corresponds with the best catalytic activity.

This strong correlation results from the decrease of the energy barrier for the interfacial electron transfer and thus facilitation of the formation of reactive surface oxygen species such as O^-, O_2, O_2^{2-} produced during the O_2 activation step responsible for soot oxidation [7,8].

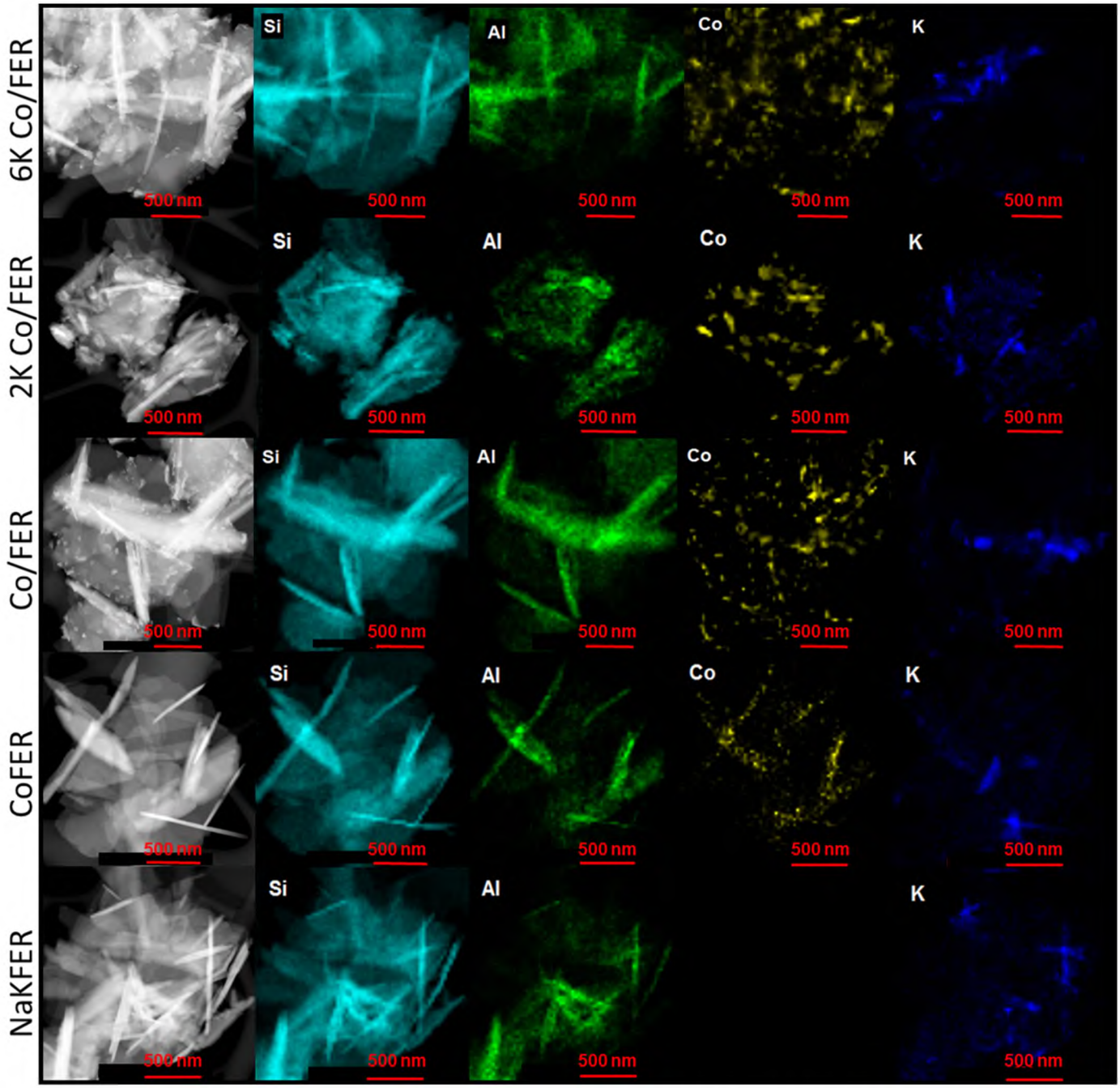

Fig. 4. STEM images together with EDX maps of Si (blue), Al (green), Co (yellow), and K (dark blue) distributions in the NaKFER, CoFER, Co/FER, 2 K Co/FER, and 6 K Co/FER samples.

3.4. The surface state of potassium studied by the species-resolved thermal alkali desorption method

In Fig. 8 the profiles of the K-desorption fluxes registered for the 2 K Co/FER, 6 K Co/FER, and 10 K Co/FER catalysts are collected. We presented the heating (red) and cooling (blue) stages of the measurement. The onset of the potassium atoms desorption is observed at 450 °C for the all studied samples. However, the courses of desorption curves vary significantly, revealing differences in the potassium surface state for these three samples.

For the 2 K Co/FER catalyst (Fig. 8A) we observed the exponential character of K atom desorption during both heating and cooling phases of the experiment; however, these two stages did not follow the same path. The desorption profile measured during the sample cooling step is shifted toward higher temperatures, which may be related to the low potassium content and desorption of the most loosely bonded fraction of the potassium species during the heating stage. For the 6 K Co/FER sample we observed the exponential character of the K desorption signal with increasing temperature and the same course for heating and cooling steps. It confirms that there is a large pool of well-dispersed potassium species without an apparent segregation (Fig. 8B). In turn, the segregation is evident for 10 K Co/FER, where a local maximum in the desorption signal is centered at approximately 500 °C, indicating the presence of a loosely bonded potassium species fraction (Fig. 8C). These results corroborate the WF changes studies indicating that the 6 K Co/FER catalyst is the optimal material in terms of the dispersion of K promoter, exhibiting a uniform surface coverage, without an appreciable segregation.

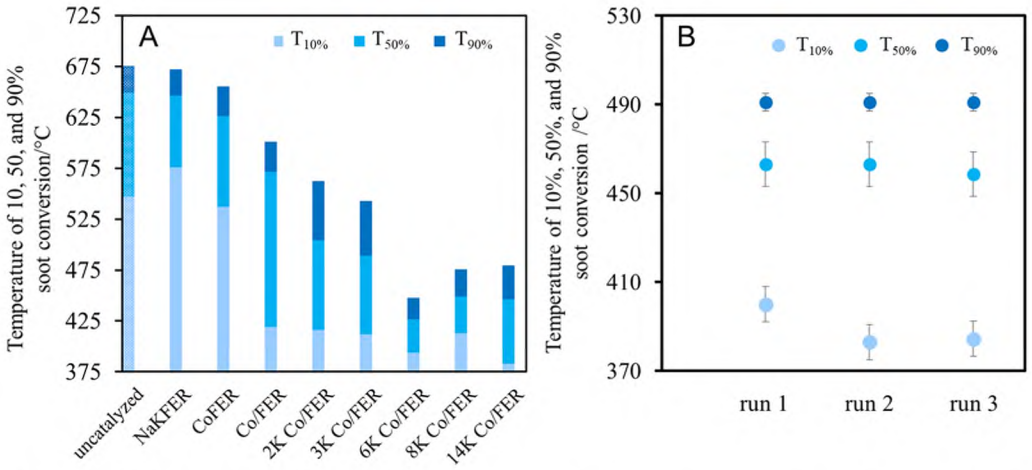

Fig. 5. Optimization of K-loading for the cobalt-based ferrierite-supported catalyst for the soot combustion reaction. A) $T_{10\%}$, $T_{50\%}$, and $T_{90\%}$ and B) stability of catalytic activity of 6 K Co/FER catalyst over three subsequent tests. Tests were performed in the tight contact mode in 5% O_2/He atmosphere with a TGA analysis.

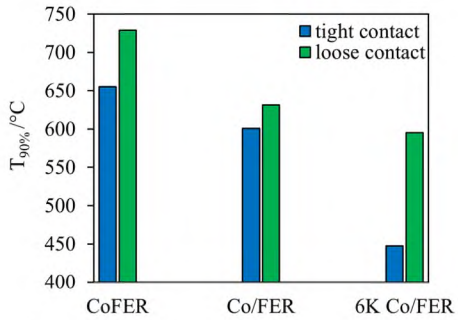

Fig. 6. Comparison of the activity in soot combustion determined as the temperature of the 90% conversion ($T_{90\%}$) for the selected catalysts: CoFER, Co/FER, and 6 K Co/FER in tight and loose contact conditions in 5% O_2/He atmosphere.

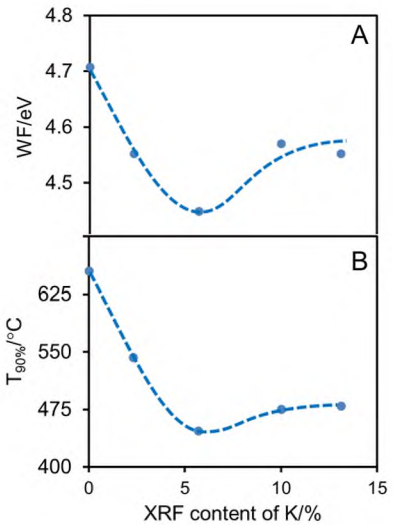

Fig. 7. Relationships between the changes of (A) the work function and (B) the catalyst activity in soot oxidation (tight contact, 5% O_2/He) expressed as $T_{90\%}$ with the potassium concentration determined from XRF studies.

3.5. *The effect of NO*

In Fig. 9 we presented the comparison of the results of the catalytic tests in loose contact mode with and without NO in the gas mixture for our best 6 K Co/FER catalyst and the undoped Co/FER catalyst.

As expected, NO addition improved the activity of the Co/FER catalyst, shifting the soot oxidation curve towards a lower temperature ($\Delta T_{10\%} \approx 75\,^{\circ}C$, $\Delta T_{50\%} \approx 70\,^{\circ}C$, $\Delta T_{90\%} \approx 40\,^{\circ}C$). Surprisingly, the presence of NO deteriorates the reaction of soot oxidation over the potassium-doped sample, 6 K Co/FER, and the higher the reaction temperature, the more significant the conversion decrease is.

To understand the observed effect we performed FT-IR and XPS spectroscopic studies for the fresh Co/FER and 6 K Co/FER catalysts and their mixtures with soot after stopping the soot combustion reaction (loose contact, 3.3% O_2/0.33% NO/He, 60 ml·min^{-1}) at the stage of 10% and 50% conversion. The temperatures, at which reactions were stopped, had been estimated based on full temperature range experiments performed previously (Fig. 9). The FT-IR spectra collected in Fig. 10 revealed that the presence of potassium influences the surface interaction with nitrate species. In the spectra of the potassium-free catalyst (Fig. 10A) we observed two bands centered at 1393 and 1375 cm^{-1} which are diagnostic for monodentate nitrates accommodated on the catalyst surface due to their incomplete decomposition during the calcination process.

Indeed, the NO_x^- species are stable at higher temperatures and their thermal stability depends on the structure and the kind of cation to which they are bonded. Judging from the intensities of the nitrate bands, we concluded their marginal accommodation on K-free samples. However, the abundance of nitrates increased for K-doped catalysts, which was accompanied by a shift of their FT-IR bands toward higher frequencies. Such behavior suggests that NO_x species are released less effectively from potassium than from cobalt sites during calcination treatment. The phenomenon of K-induced accommodation of nitrates on the catalyst surface is visible for the catalysts when NO is present in the gas stream. During the oxidation of soot by a mixture of O_2 and NO stable nitrate species are formed. Furthermore, the upshift of the nitrate bands indicates a privileged location of NOx^- formed at the K sites: for the 6 K Co/FER sample, the nitrate bands are located at higher frequencies (1412 and 1390 cm^{-1}). Based on the literature these bands were attributed mainly to monodentate nitrates bonded to K^+ cations [42]. The high thermal stability of nitrates formed on K-enriched surfaces results in a deterioration of catalytic activity, which is most likely related to blocking the active centers of the catalyst [28] and canceling the electronic promotion effect due to K doping.

Similarly, an *ex situ* XPS analysis was performed to determine the

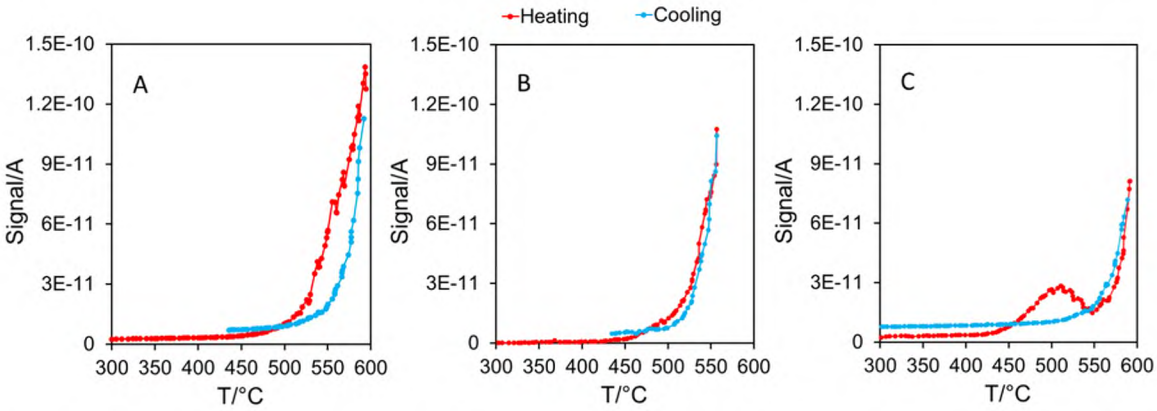

Fig. 8. Potassium thermal desorption signals corresponding to heating (red points) and cooling (blue points) of the 2 K Co/FER, 6 K Co/FER, and 10 K Co/FER catalysts.

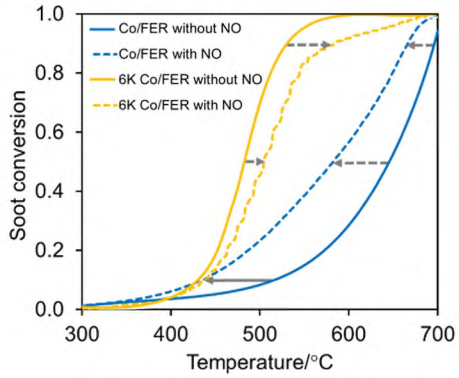

Fig. 9. The effect of NO presence in the feed on the Co/FER and 6 K Co/FER catalysts activity in the soot combustion reaction in loose contact mode.

surface composition of the catalyst/soot mixture at 10% and 50% of the soot oxidation reaction stages (see Figs. S4-S6). The same two catalysts were investigated; Co/FER and potassium-promoted 6 K Co/FER. Fresh samples, without soot, were used as references. Mixing with soot leads to covering of the whole Co/FER catalyst surface (decrease of surface concentration of all elements except carbon, Fig. 11 A and B). An increase in the oxidation of soot from 10% to 50% does not change appreciably the surface composition of the mixture. At the same time, the nitrogen atomic concentration remains at the background level for all three samples (Fig. 11 B). The constant composition of the catalyst/soot mixture may result from a uniform, non-preferential soot oxidation over the entire catalyst surface. Similarly to the non-K-promoted samples, mixing with soot leads to covering of the 6 K Co/FER catalyst surface (decrease of surface concentration of all elements but carbon, Fig. 11 C and D). However, in contrast, an increase in soot oxidation from 10% to 50% leads to an increase in the surface concentration of all catalyst components but K and a decrease in the surface concentration of carbon. Furthermore, the atomic nitrogen concentration increases in the samples after the partial oxidation of soot, indicating the formation of nitrates (Fig. 11 D). A decrease in carbon content in the catalyst/soot mixture results from preferential oxidation of the soot over the potassium-promoted active centers and uncovering the catalyst surface.

We hypothesize that the decrease in the potassium content results from the diffusion of potassium on the surface and into the soot particles, enhancing their combustion. Although the thermal mobility of potassium, shown in Fig. 8, indicates that K desorption detected with the SR-TAD apparatus starts already at 450 °C, additional experimental studies to confirm this hypothesis should be performed.

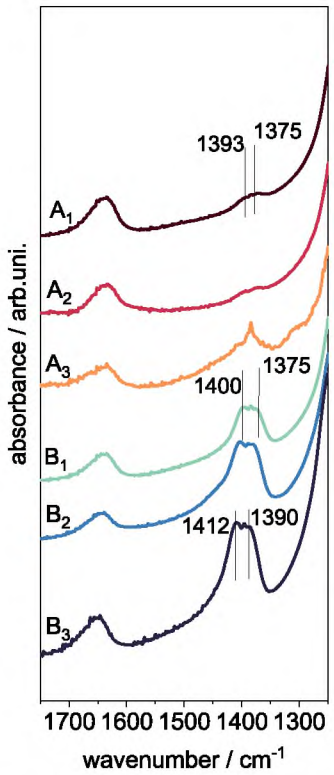

Fig. 10. FT-IR spectra collected in KBr of Co/FER (A) and 6 K Co/FER (B) catalysts at different stages (0% conversion (A_1, B_1), 10% conversion (A_2, B_2), and 50% conversion (A_3, B_3) of soot combustion reaction in loose contact mode with NO in the gas flow.

4. Conclusions

The results of this research revealed that careful adjustment of potassium promotion can lead to a promising cobalt catalyst for the soot oxidation reaction based on the economically and environmentally friendly ferrierite. Although our catalyst is not reaching the activity level of Pt-based materials, it provides a very good starting point to develop a new class of eco-catalysts based on zeolites. The catalytic activity of K-doped Co/FER catalyst strongly depends on potassium content. $T_{90\%}$ decreases with K loading, reaches the minimum for 6 K Co/FER, and increases slightly again for 10 K Co/FER and 14 K Co/FER. The 90% conversion of soot for optimal 6 K Co/FER was achieved at a temperature below 450 °C. The strong correlation between the work function

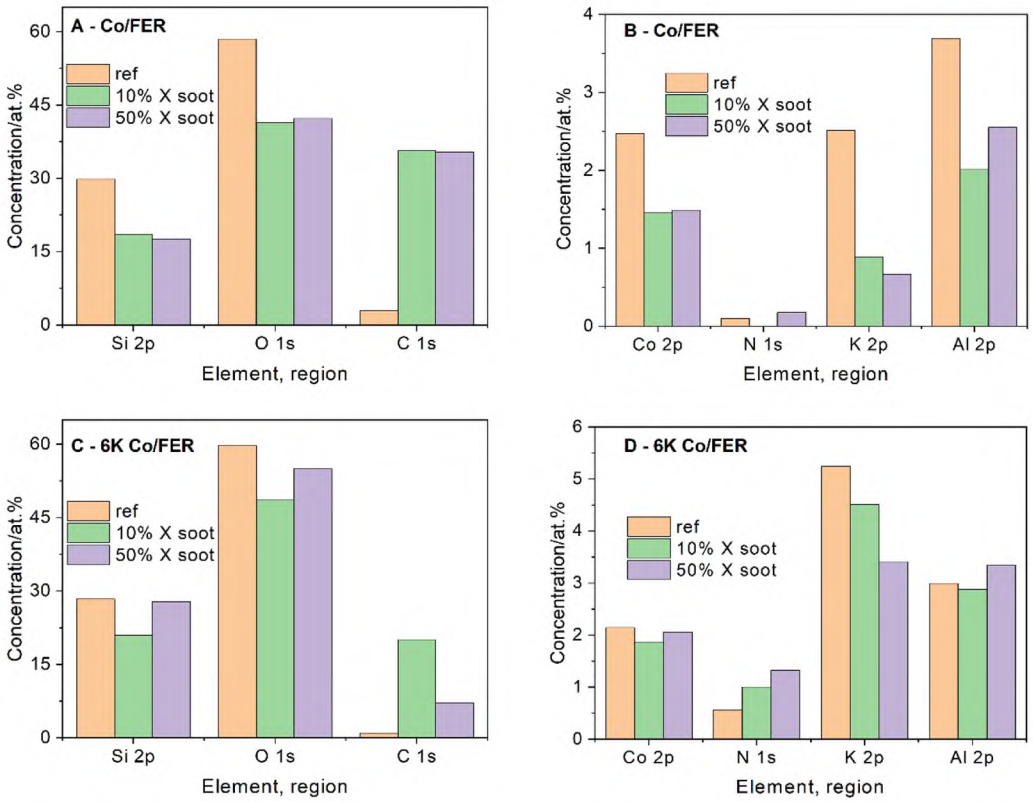

Fig. 11. Quantification of the surface composition of the catalyst/soot mixture at 10% and 50% of the soot oxidation reaction stages for Co/FER A) Si, O, C; B) Co, N, K, Al, and 6 K Co/FER C) Si, O, C; D) Co, N, K, Al.

measured with the Kelvin method and the activity in soot oxidation revealed the electronic character of K doping. Furthermore, the studies of the surface state of potassium by SR-TAD method confirmed optimal potassium dispersion for optimized 6 K Co/FER catalyst and potassium overloading for 10 K Co/FER sample. These unique surface state studies allowed us to confirm that optimal potassium promoter dispersion correlates with the optimized electronic properties of the K-doped Co-FER catalyst and its catalytic activity.

The presence of NO deteriorates the catalytic activity of the K-doped sample, in contrast to the frequently reported positive effect of NO addition. In-depth spectroscopic studies of the catalysts' surfaces at different stages of the soot oxidation reaction indicated that the opposite effect of NO for K-doped and undoped catalysts is caused by an enhanced formation of nitrate species on the surface of the K-containing catalyst.

This research opens a new class of catalytic supports for soot oxidation catalysis. Although the applied zeolite support is completely catalytically inactive, the reactive zeolite-supported catalysts can be successfully developed.

CRediT authorship contribution statement

GG: Conceptualization, Methodology, Investigation, Writing – original draft, Writing – review & editing, Supervision, Project administration, Funding acquisition. **MR**: Investigation, Data curation. **KGM:** FT-IR investigation and data analysis, Resources, Writing – review & editing. **PS**: XPS data analysis, Writing – review & editing. **GS**: Investigation, Data curation. **AK:** Resources, Writing – review & editing. All authors have read and agreed to the published version of the manuscript.

Declaration of Competing Interest

The authors declare that they have no known competing financial interests or personal relationships that could have appeared to influence the work reported in this paper.

Data availability

Data will be made available on request.

Acknowledgment

The work was financed by Grant No. 2021/43/D/ST4/03016 from the National Science Centre, Poland.

Appendix A. Supporting information

Supplementary data associated with this article can be found in the online version at doi:10.1016/j.apcata.2023.119469.

References

[1] European Environmental Agency, Air Quality in Europe–2020 Report, Copenhagen, Denmark, 2020.
[2] X. Zhou, H. Zhang, Y. Sun, Z. Gao, H. Chen, Fuel 351 (2023), 128805.
[3] S. Liu, X. Wu, H. Luo, D. Weng, R. Ran, Pt/Zeolite catalysts for soot oxidation: influence of hydrothermal aging, J. Phys. Chem. C. 119 (2015) 17218–17227.
[4] S. Liu, X. Wu, D. Weng, M. Li, R. Ran, Roles of acid sites on Pt/H-ZSM5 catalyst in catalytic oxidation of diesel soot, ACS Catal. 5 (2015) 909–919.
[5] A.M. Hernández-Giménez, D.L. Castelló, A. Bueno-López, Diesel soot combustion catalysts: review of active phases, Chem. Pap. 68 (2014) 1154–1168.
[6] S. Liu, X. Wu, D. Weng, R. Ran, Ceria-based catalysts for soot oxidation: a review, J. Rare Earths 33 (2015) 567–590.
[7] P. Legutko, P. Stelmachowski, X. Yu, Z. Zhao, Z. Sojka, A. Kotarba, Catalytic Soot Combustion—General Concepts and Alkali Promotion, ACS Catal. 13 (2023) 3395–3418.
[8] L. Chen, T. Li, J. Zhang, J. Wang, P. Chen, M. Fu, J. Wu, D. Ye, Chemisorbed superoxide species enhanced the high catalytic performance of Ag/Co_3O_4 nanocubes for soot oxidation, ACS Appl. Mater. Interfaces 13 (2021) 21436–21449.
[9] P. Zhang, M. Yang, D. Han, X. Liu, X. Yu, J. Xiong, Y. Li, Z. Zhao, J. Liu, Y. Wei, Synergistic integration of energy storage catalysis: a multifunctional catalytic

material for round-the-clock environmental cleaning, Appl. Catal. B Environ. 321 (2023), 122077.
[10] Y. Li, T. Qin, Y. Ma, J. Xiong, P. Zhang, K. Lai, X. Liu, Z. Zhao, J. Liu, L. Chen, Y. Wei, Revealing active edge sites induced by oriented lattice bending of Co-CeO_2 nanosheets for boosting auto-exhaust soot oxidation, J. Catal. 421 (2023) 351–364.
[11] P. Zhang, X. Mei, X. Zhao, J. Xiong, Y. Li, Z. Zhao, Y. Wei, Boosting catalytic purification of soot particles over double perovskite-type $La_{2-x}K_xNiCoO_6$ catalysts with an ordered macroporous structure, Environ. Sci. Technol. 55 (2021) 11245–11254.
[12] H. Liang, S. Wu, Y. Hong, S. Li, Y. Chen, X. Yu, D. Ye, Influence of alkali metals with different ionic radius doping into $Ce_{0.7}Zr_{0.3}O_2$ on the active oxygen, Catal. Lett. 144 (2014) 685–690.
[13] R. Matarrese, E. Aneggi, L. Castoldi, J. Llorca, A. Trovarelli, L. Lietti, Simultaneous removal of soot and NO over K- and Ba-doped ruthenium supported catalysts, Catal. Today 267 (2016) 119–129.
[14] P. Legutko, P. Stelmachowski, M. Trębala, Z. Sojka, A. Kotarba, Role of electronic factor in soot oxidation process over tunnelled and layered potassium iron oxide catalysts, Top. Catal. 56 (2013) 489–492.
[15] P. Legutko, W. Kaspera, P. Stelmachowski, Z. Sojka, A. Kotarba, Boosting the catalytic activity of magnetite in soot oxidation by surface alkali promotion, Catal. Commun. 56 (2014) 139–142.
[16] P. Legutko, T. Jakubek, W. Kaspera, P. Stelmachowski, Z. Sojka, A. Kotarba, Soot oxidation over K-doped manganese and iron spinels — How potassium precursor nature and doping level change the catalyst activity, Catal. Commun. 43 (2014) 34–37.
[17] E.E. Bickel, C.T. Nimlos, R. Gounder, Developing quantitative synthesis-structure-function relations for framework aluminum arrangement effects in zeolite acid catalysis, J. Catal. 399 (2021) 75–85.
[18] I. Borthakur, A. Sau, S. Kundu, Cobalt-catalyzed dehydrogenative functionalization of alcohols: progress and future prospect, Coord. Chem. Rev. 451 (2022), 214257.
[19] Y. Li, L. Li, J. Yu, Applications of zeolites in sustainable chemistry, Chem 3 (2017) 928–949.
[20] M. Moshoeshoe, M. Silas Nadiye-Tabbiruka, V. Obuseng, Am. J. Mater. Sci. 2017 (2017) 196–221.
[21] Q. Zhang, J. Yu, A. Corma, Applications of Zeolites to C1 Chemistry: Recent Advances, Challenges and Opportunities, Adv. Mater. 32 (2020), 2002927.
[22] J. Van der Mynsbrugge, A.T. Bell, Challenges for the theoretical description of the mechanism and kinetics of reactions catalyzed by zeolites, J. Catal. 404 (2021) 832–849.
[23] T.T. Le, A. Chawla, J.D. Rimer, Impact of acid site speciation and spatial gradients on zeolite catalysis, J. Catal. 391 (2020) 56–68.
[24] C.H.F. Peden, Cu/Chabazite catalysts for 'Lean-Burn' vehicle emission control, J. Catal. 373 (2019) 384–389.
[25] T.F. Degnan Jr., Applications of zeolites in petroleum refining, Top. Catal. 13 (2000) 349–356.
[26] J. Xu, X. Xiao, S. Zeng, M. Cai, M.W. Verbrugge, Synergistic combination of two antimicrobial agents closing each other's mutant selection windows to prevent antimicrobial resistance, ACS Appl. Energy Mater. 1 (2018) 7237–7243.
[27] G. Grzybek, M. Greluk, P. Patulski, P. Stelmachowski, K. Tarach, G. Słowik, M. Rotko, S. Valencia, F. Rey, K. Góra-Marek, Adjustment of the ZSM-5 zeolite support towards the efficient hydrogen production by ethanol steam reforming on cobalt catalysts, Chem. Eng. J. 467 (2023), 143239.
[28] C. Cao, H. Yang, J. Xiao, X. Yang, B. Ren, L. Xu, G. Liu, X. Li, Catalytic diesel soot elimination over potassium promoted transition metal oxide (Co/Mn/Fe) nanosheets monolithic catalysts, Fuel 305 (2021), 121446.
[29] G. Grzybek, K. Góra-Marek, P. Patulski, M. Greluk, M. Rotko, G. Słowik, A. Kotarba, Optimization of the potassium promotion of the Co|α-Al_2O_3 catalyst for the effective hydrogen production via ethanol steam reforming, Appl. Catal. A Gen. 614 (2021), 118051.
[30] G. Grzybek, M. Greluk, K. Tarach, K. Pyra, G. Słowik, M. Rotko, K. Góra-Marek, Bioethanol steam reforming over cobalt-containing USY and ZSM-5 commercial zeolite catalysts, Front. Mater. 7 (2020), 597528.
[31] G. Słowik, M. Greluk, A. Machocki, Microscopic characterization of changes in the structure of KCo/CeO_2 catalyst used in the steam reforming of ethanol, Mater. Chem. Phys. 173 (2016) 219–237.
[32] N. Fairley, V. Fernandez, M. Richard-Plouet, C. Guillot-Deudon, J. Walton, E. Smith, D. Flahaut, M. Greiner, M. Biesinger, S. Tougaard, D. Morgan, J. Baltrusaitis, Systematic and collaborative approach to problem solving using X-ray photoelectron spectroscopy, Appl. Surf. Sci. Adv. 5 (2021), 100112.
[33] B. Ura, J. Trawczyński, A. Kotarba, W. Bieniasz, M.J. Illán-Gómez, A. Bueno-López, F.E. López-Suárez, Effect of potassium addition on catalytic activity of $SrTiO_3$ catalyst for diesel soot combustion, Appl. Catal. B Environ. 101 (2011) 169–175.
[34] G. Grzybek, S. Wójcik, P. Legutko, J. Gryboś, P. Indyka, B. Leszczyński, A. Kotarba, Z. Sojka, Thermal stability and repartition of potassium promoter between the support and active phase in the K-$Co_{2.6}Zn_{0.4}O_4$|α-Al_2O_3 catalyst for N_2O decomposition: crucial role of activation temperature on catalytic performance, Appl. Catal. B Environ. 205 (2017) 597–604.
[35] G. Grzybek, M. Greluk, P. Indyka, K. Góra-Marek, P. Legutko, G. Słowik, S. Turczyniak-Surdacka, M. Rotko, Z. Sojka, A. Kotarba, Cobalt catalyst for steam reforming of ethanol–Insights into the promotional role of potassium, Int. J. Hydrog. Energy 5 45 (2020) 22658–22673.
[36] G. Grzybek, K. Góra-Marek, K. Tarach, K. Pyra, P. Patulski, M. Greluk, G. Słowik, M. Rotko, A. Kotarba, Tuning the properties of the cobalt-zeolite nanocomposite catalyst by potassium: Switching between dehydration and dehydrogenation of ethanol, J. Catal. 407 (2022) 364–380.
[37] G. Grzybek, K. Ciura, S. Wójcik, J. Gryboś, P. Indyka, M. Inger, K. Antoniak-Jurak, P. Kowalik, A. Kotarba, Z. Sojka, On the selection of the best polymorph of Al_2O_3 carriers for supported cobalt nano-spinel catalysts for N_2O abatement: an interplay between preferable surface spreading and damaging active phase–support interaction, Catal. Sci. Technol. 7 (2017) 5723–5732.
[38] R. García, L. Gómez-Hortigüela, I. Díaz, E. Sastre, J. Pérez-Pariente, Synthesis of materials containing ferrierite layers using quinuclidine and 1-benzyl-1-methyl-pyrrolidine as structure-directing agents. An experimental and computational study, Chem. Mater. 20 (2008) 1099–1107.
[39] N. Kanno, M. Miyake, M. Sato, Syntheses of ferrierite, ZSM-48, and ZSM-5 in glycerol solvent, Zeolites 14 (1994) 625–628.
[40] S. Teketel, L.F. Lundegaard, W. Skistad, S.M. Chavan, U. Olsbye, K.P. Lillerud, P. Beato, S. Svelle, Morphology-induced shape selectivity in zeolite catalysis, J. Catal. 327 (2015) 22–32.
[41] H.S. Jung, F. Zafar, X. Wang, T.X. Nguyen, C.H. Hong, Y.G. Hur, J.W. Choung, M. J. Park, J.W. Bae, Morphology effects of ferrierite on bifunctional Cu–ZnO–Al_2O_3/ferrierite for direct syngas conversion to dimethyl ether, ACS Catal. 11 (2021) 14210–14223.
[42] K.I. Hadjiivanov, Identification of neutral and charged N_xO_y surface species by IR spectroscopy, Catal. Rev. - Sci. Eng. 42 (2000) 71–144.